Published in final edited form as:

Neuroimage. 2025 May 15; 312: 121211. doi:10.1016/j.neuroimage.2025.121211.

Comparison of structural connectomes for modeling deep brain stimulation pathway activation

Ketan Mehta[a], **Angela M. Noecker**[a], **Cameron C. McIntyre**[a,b,*]

[a]Department of Biomedical Engineering, Duke University, Durham, NC, United States

[b]Department of Neurosurgery, Duke University, Durham, NC, United States

Abstract

Introduction: Structural connectivity models of the brain are commonly employed to identify pathways that are directly activated during deep brain stimulation (DBS). However, various connectomes differ in the technical parameters, parcellation schemes, and methodological approaches used in their construction.

Objective: The goal of this study was to compare and quantify variability in DBS pathway activation predictions when using different structural connectomes, while using identical electrode placements and stimulation volumes in the brain.

Approach: We analyzed four example structural connectomes: 1) Horn normative connectome (whole brain), 2) Yeh population-averaged tract-to-region pathway atlas (whole brain), 3) Petersen histology-based pathway atlas (subthalamic focused), and 4) Majtanik histology-based pathway atlas (anterior thalamus focused). DBS simulations were performed with each connectome, at four

*Corresponding author at: Duke University, Hudson Hall, Room 135, 101 Science Drive, Durham, NC 27708, United States, cameron.mcintyre@duke.edu (C.C. McIntyre).

Ethics statement

The research presented in this article is original work by the authors. Datasets utilized in this study were derived from the following resources available in the public domain: Horn structural group connectome of 32 adult diffusion MGH-USC HCP subjects (https://www.lead-dbs.org/helpsupport/knowledge-base/atlasesresources/normative-connectomes/); Yeh HCP 1065 population-averaged tractography atlas (https://brain.labsolver.org/hcp_trk_atlas.html); Petersen pathway atlas (https://osf.io/mhd4z/). The Majtanik pathway atlas is not publicly available, but was provided by the original authors (Majtanik et al., 2022) upon request. Ethical approval and informed consent for data collection were handled by the original data providers. No new human data was collected specifically for this study, and all conducted analyses strictly adhered to the protocols and guidelines established by the original data providers.

CRediT authorship contribution statement

Ketan Mehta: Writing – review & editing, Writing – original draft, Software, Methodology, Investigation, Formal analysis, Data curation. **Angela M. Noecker:** Writing – review & editing, Writing – original draft, Visualization, Software, Methodology, Investigation. **Cameron C. McIntyre:** Writing – review & editing, Writing – original draft, Supervision, Project administration, Methodology, Funding acquisition, Conceptualization.

Declaration of competing interest

CCM is a paid consultant for Boston Scientific Neuromodulation, receives royalties from Hologram Consultants, Neuros Medical, Qr8 Health, Ceraxis Health, and is a shareholder in the following companies: Hologram Consultants, BrainDynamics, Surgical Information Sciences, CereGate, Cardionomic, Enspire DBS. AMN is a paid consultant and shareholder in Hologram Consultants. KM has no conflicts of interest to disclose.

Supplementary materials

Supplementary material associated with this article can be found, in the online version, at doi:10.1016/j.neuroimage.2025.121211.

generalized locations for DBS electrode placement: 1) subthalamic nucleus, 2) anterior nucleus of thalamus, 3) ventral capsule, and 4) ventral intermediate nucleus of thalamus.

Results: The choice of connectome used in the simulations resulted in notably distinct pathway activation predictions, and quantitative analysis indicated little congruence in the predicted patterns of brain network connectivity. The Horn and Yeh tractography-based connectomes provided estimates of DBS connectivity for any stimulation location in the brain, but have limitations in their anatomical validity. The Petersen and Majtanik histology-based connectomes are more anatomically realistic, but are only applicable to specific DBS targets because of their limited representation of pathways.

Significance: The widely varying and inconsistent inferences of DBS network connectivity raises substantial concern regarding the general reliability of connectomic DBS studies, especially those that lack anatomical and/or electrophysiological validation in their analyses.

Keywords

Connectomic; Atlas; Normative; Subthalamic nucleus; Thalamus; Ventral capsule

1. Introduction

Deep brain stimulation (DBS) is an established therapy for the treatment of movement disorders (Krack et al., 2019). Clinical use of DBS is also growing in the treatment of epilepsy (Fisher et al., 2010), and long-standing research efforts are working to create DBS therapies for neuropsychiatric disorders (Hitti et al., 2023). One key to the effectiveness of DBS is its ability to act on focal subcortical targets, but modulate neural circuits throughout the brain (Rosenberg, 2015). As such, a growing trend in DBS research is to use axonal pathway activation modeling to identify the specific brain network connections that are modulated during stimulation (Chaturvedi et al., 2010; Lujan et al., 2012). Associating these activated pathways with the generation of a specific therapeutic effect (or adverse effect) has utility for DBS neurosurgical targeting (Noecker et al., 2018), device programming (Hines et al., 2024), and mechanistic analyses (Howell et al., 2021; Seas et al., 2024). This direction of DBS research is facilitated by parallel advances in neuroinformatics and neuroimaging techniques that enable the development of structural brain connectomes, and is often referred to as connectomic DBS modeling (Neudorfer et al., 2023).

There are two general approaches to defining structural connectomes used in DBS analyses, which consist of either using patient-specific data or using a reference atlas of pathways. In the patient-specific approach, diffusion weighted imaging (DWI) data is collected for each patient. That data is then processed using a tractography algorithm to estimate streamlines and construct an individualized map of their structural connectivity. In contrast, the reference atlas approach relies on using a pre-defined connectomic model consisting of streamlines that were created within an atlas brain. The connectomic atlas can then be non-linearly warped to fit the MRI of a *de novo* subject to provide a semi-patient-specific representation of the brain connectome.

Most early connectomic DBS studies focused on using patient-specific tractography approaches (Akram et al., 2017; Chaturvedi et al., 2010; Howell et al., 2019). However, this strategy limits analyses to patients that have pre-operative DWI data, which is not always available, and there is an ongoing debate about the quality of pathway reconstructions that can be made with clinical-grade DWI data (Petersen and McIntyre, 2023). Therefore, the majority of recent connectomic DBS studies have focused on using connectomic atlases. The appeal of connectomic atlases is their speed and simplicity. They can also potentially provide pathway estimates that have a higher degree of anatomical realism when compared to tractographic algorithms, which can struggle in focal brain regions with tortuous and crisscrossing trajectories (Petersen et al., 2019). In addition, the use of connectomic atlases help to facilitate population-based statistical analyses and group-level inferences (Neudorfer et al., 2023).

While connectomic atlases serve as models of brain connectivity, individual atlas options vary in the technical parameters of their construction, parcellation schemes, and level of anatomical annotation. For example, normative connectomes (Elias et al., 2022; Horn et al., 2017) are composed of millions of streamlines without any anatomical labeling and essentially serve as population-averaged whole brain tractograms. Alternatively, large-scale pathway atlases (Radwan et al., 2022; Yeh, 2022; Zhang et al., 2018) organize and segment tractography streamlines into annotated white matter bundles. Meanwhile, histology-based pathway atlases (Adil et al., 2021; Majtanik et al., 2022; Petersen et al., 2019) incorporate traditional anatomical datasets to more accurately map pathways in focal brain regions. Previous studies have analyzed the variability in pathway estimation due to differences in image acquisition (Maier-Hein et al., 2017), tractographic algorithm (Schilling et al., 2021), and reconstruction methodology (Petersen and McIntyre, 2023). However, variability in the predicted pathway activation to DBS in different connectomes remains to be fully investigated.

The goal of this study was to provide a side-by-side comparison of connectomic DBS simulations from different connectomic atlases in a variety of DBS targets. In particular, we quantified and compared variations in the predicted DBS pathway activation when using four popular connectomic atlases, using identical DBS electrode placements and stimulation volumes in the brain. The results reveal that the choice of connectome has a major impact on the predicted pattern of DBS network connectivity, and highlights some of the many caveats associated with connectomic DBS analyses.

2. Methods

2.1. Connectomic atlases

The analyses focus on four popular, yet characteristically different, structural connectomic atlases. The Horn normative connectome (Horn et al., 2017), derived from healthy young subjects of the Human Connectome Project (HCP) (Setsompop et al., 2013). The Yeh HCP1065 population-averaged tract-to-region atlas (Yeh, 2022), derived from healthy young HCP subjects (Yeh et al., 2018). The Petersen histology-based pathway atlas (Petersen et al., 2019), specifically designed to represent the subhtalamic nucleus (STN) region. The Majtanik histology-based pathway atlas (Majtanik et al., 2022), specifically designed to

represent the anterior nucleus of thalamus (ANT) region. The characteristic features of each atlas are summarized in Table 1.

To allow for a direct and consistent comparison across atlases, streamlines from every atlas were preprocessed by first converting them from their natively available software formats (Table 1) into *.vtk* polygonal data format, which is compatible with StimVision (Noecker et al., 2021). Format conversion was performed using custom written Python scripts, to ensure that the streamline integrity was completely preserved during conversion. The streamlines were then non-linearly warped and registered to the high-resolution (0.7 mm isotropic voxels) CIT168 (Pauli et al., 2018) standard reference brain using Advanced Normalization Tools (ANTs) (Avants et al., 2011). Finally, we restricted our analysis to the left hemisphere of the brain, and correspondingly reduced the total number of streamlines within each connectomic dataset (Table 1) by discarding any streamlines not within the left hemisphere.

2.2. Connectomic DBS simulations

We considered four clinically relevant locations (Table 2) for DBS electrode placement in the left hemisphere of the brain: 1) subthalamic nucleus (STN), 2) ventral capsule (VC), 3) anterior nucleus of thalamus (ANT), and 4) ventral intermediate nucleus of thalamus (VIM). These location choices correspond to commonly used surgical targets for DBS in the treatment of Parkinson's disease, epilepsy, obsessive-compulsive disorder, and tremor, respectively (Fig. 1). DBS at the different surgical targets was simulated using StimVision (Noecker et al., 2021).

There are many different methods for estimating the "volume of tissue activated" by DBS as a function of the stimulation parameter settings (Butson and McIntyre, 2006). However, the nuances of those differences have been covered elsewhere (Gunalan et al., 2018) and are not directly relevant to the differences in connectomes. Therefore, to perform the simplest comparison of connectomes possible we elected to use generic spheres to represent activation volumes around the DBS electrode. Results are presented with activation spheres centered on the 2nd level of contacts on a 2202 DBS electrode (Boston Scientific).

Streamline activation was estimated at each target location, with each connectomic atlas, using overlap with a range of spherical activation volumes (Fig. 1). The center of each activation sphere was coincident with the center of the active contacts of the electrode, while the radius of the sphere was linearly increased from 0.5 mm to 6 mm. A streamline was categorized as activated if it passed through the activation sphere. For general reference, activation spheres of radii 2 mm or 5 mm would be loosely representative of the stimulus spread associated with ~3 mA, 60 μs or ~7 mA, 60 μs monopolar (cathodic) DBS, respectively (Gunalan et al., 2018).

Our streamline activation estimates incorporated realistic levels of uncertainty with regard to DBS electrode positioning at each target location (i.e., STN, VC, ANT, VIM). To simulate positional uncertainty, we moved the DBS electrode around the stimulation site (Table 2, Fig. 1d) in a 3 × 3 × 3 cubic grid pattern with 27 points, each spaced 1 mm apart from each other (Bower et al., 2023). For each activation sphere radius evaluated, streamline activation at each target location was calculated 27 times by successively moving the center of the

sphere to each corresponding point on the grid. The overall percentage of pathway activation at a given target location was then calculated by averaging the streamline activation count across all 27 points, and dividing it by the total number of streamlines in the connectome. The specific pathway activation percentage was similarly calculated by dividing the average (across all 27 points) number of activated streamlines within a given annotated pathway by the total number of streamlines within that pathway. Finally, recruitment curves were constructed for each target location by incrementally increasing the radius of the activation sphere from 0.5 to 6.0 mm (in steps of 0.5 mm), and recording the resultant percentage activation at the given radius.

2.3. Estimating connectivity profiles

To facilitate a standardized comparison of DBS connectivity across connectomes, we parcellated the left hemisphere cortex of the CIT168 brain into 34 regions of interest (ROI) (supplementary Fig. S1) using the Desikan-Killiany cortical atlas (Desikan et al., 2006). Parcellation was performed using the automated volumetric segmentation tool in FreeSurfer (Fischl, 2012), allowing each voxel in the cortex to be assigned a corresponding ROI label.

For a given activation sphere, connectivity between the DBS target (i.e., STN, VC, ANT, VIM) and a cortical ROI was determined by checking if either endpoint of an activated streamline terminated within that ROI. A frequency distribution was generated by counting the number of activated streamlines terminating at each ROI. The proportion of streamlines projecting to each ROI was calculated by dividing the frequency counts within the distribution by the total number of activated streamlines. Finally, activation-dependent connectivity profiles for each target location were constructed by repeating this process using the activation spheres at each of 27 points (on the cubic grid) as a seed, and then taking the average (across all 27 points) proportion of activated streamlines projecting to each ROI.

2.4. Quantifying variability in DBS connectivity

For quantitative analyses, we employed four different statistical measures to compare the variability in pathway activation across the connectomes at each DBS target. These measures include: 1) the volume-based Dice overlap coefficient (Dice, 1945), 2) the streamline-based bundle adjacency score (Chandio et al., 2020), 3) the Jensen-Shannon information-theoretic distance metric (Endres and Schindelin, 2003), and 4) the weighted degree centrality (Candeloro et al., 2016).

The Dice overlap coefficient was used to measure overall volume similarity between activated streamlines based on voxel overlap. Dice overlap is a common evaluation metric for measuring the similarity between two sets (bundles) of streamlines (Rheault et al., 2020; Schilling et al., 2021), and is equal to twice the intersection of the two sets divided by the sum of the sizes of the two sets. Dice overlap was calculated by converting the streamlines into their voxel representation (i.e. a binarized mapping of all voxels that contain a streamline) which was done using ‘density_map()’ function of the DIPY Python library (Garyfallidis et al., 2014). The volume Dice overlap is a value between 0 and 1, where 1 indicates perfect overlap and 0 no overlap.

Bundle adjacency measures shape similarity between two sets of streamlines, based on the average distance between the streamlines in each set (Chandio et al., 2020; Garyfallidis et al., 2012). Given two streamline sets X and Y, a streamline in set X is considered to be 'adjacent' to set Y, if there is at least one streamline in Y that is closer than a threshold distance $\theta > 0$ mm. The distance is calculated using all points on the streamlines, thus factoring in the overall length and trajectory of the streamlines. The bundle adjacency score ranges between 0 and 1, with a lower score indicating lower shape similarity. The score is 0 when no streamlines in either set X or Y are adjacent to each other, and 1 when they are all adjacent. The results presented in our analysis use a threshold distance of $\theta = 6$ mm, which equals the maximum radius of the activation sphere.

Jensen-Shannon distance (JSD) was used to measure the similarity between a pair of connectivity profile distributions. JSD is a measure of symmetric divergence between two probability distributions, and equals the square root of the Jensen-Shannon divergence (Lin, 1991; Nielsen, 2019). JSD is applicable for categorical distributions, even when some probabilities are zero, making it well suited for comparing the cortical connectivity profiles. JSD is also bounded between 0 and 1, with a value of 1 when the two distributions are disjoint, and 0 when the two distributions are identical. Note that for easier readability alongside the other similarity measures used in this work, we report the 1-JSD value (i.e. smaller values indicate greater dissimilarity). The Fisher's exact test was used to test for statistical significance under the null hypothesis that there is no difference between the two distributions (i.e. distribution of streamlines across the ROIs is the same for the two connectomes being compared). The p-value was computed using the 'fisher.test()' function in R (https://www.R-project.org/), using a Monte Carlo simulation with 10,000 replications.

The weighted degree centrality (WDC) metric (Candeloro et al., 2016) was used to measure the overall cortical connectivity of a DBS target within each connectome variant. WDC measures how "well--connected" a DBS target is by assigning it a score based on 1) the number of ROIs it connects to, and 2) the distribution of streamlines across the connecting ROIs. WDC is calculated by treating the DBS target location and ROIs as nodes on a network, and the proportion of activated streamlines projecting to the ROIs as connection weights. The WDC score equals the number of direct connections when the weights are uniformly distributed, and proportionately reduces as the weight distribution shifts away from uniform. A simple example illustrating the application and utility of WDC to measure the connectivity of a DBS target is provided in supplementary materials (Fig. S2).

3. Results

3.1. Pathway activation across connectomes

This study compared variations in the DBS pathway activation as predicted by the Horn, Yeh, Petersen, and Majtanik connectomes, respectively. To isolate other factors of variation in the DBS model, electrode locations and stimulation volumes were kept constant across each example connectomic atlas. Fig. 2 provides a visual example of the activated streamlines predicted with the different connectomes at the different target locations, all using an identical 3 mm radius activation sphere at the central stimulation site for each DBS target (Table 2). Side-by-side comparison of the DBS predictions highlight the variations in

the trajectory, density, and connectivity of the activated streamlines within each connectome, across the various DBS targets. The diversity and extent of pathway activation differences are quantified in the pathway recruitment curves (Fig. 3). The results demonstrate that the variations persisted for activation spheres of every size (0.5 to 6 mm). A similar side-by-side visualization comparing streamline activation for a 5 mm radius activation sphere is provided in supplementary materials (Fig. S3).

The Horn connectome exhibited wide-ranging streamline activation at all DBS locations, but the lack of anatomically defined tracts adds a layer of challenge in inferring the activated connectivity. The Yeh connectome provided estimates of whole-brain connectivity from DBS at any location with annotated pathway designations, but lacks finer anatomical details. The Petersen connectome was only applicable to the STN, VC, and VIM targets because of its limited representation of pathways, while the Majtanik connectome was similarly only applicable to the ANT target. The histology-based connectomes (Petersen and Majtanik) also had a significantly higher percentage of pathway activation for the same stimulation volume (Fig. 3), but given the relative differences in the size of each connectome, the number of streamlines activated within each connectome remained comparable. For example, a 3 mm activation sphere in the STN had an average streamline activation count of 5090±1488, 1094±202, and 1584±214, for the Horn, Yeh, and Petersen connectomes, respectively.

Visual inspection of the activated streamlines across the different connectomes suggests that STN DBS connectivity exhibits the greatest discrepancies. For example, the tractography-based connectomes (Horn and Yeh) exhibit a strong anterior projection bias in their representation of the posterior limb of the internal capsule (Fig. 2). However, these trajectories are not consistent with anatomically documented connectivity of the motor system with the subthalamic region (Archer et al., 2018; Petersen et al., 2019; Plantinga et al., 2018). In addition, finer details associated with activating smaller pathways within the basal ganglia are available with the Petersen connectome, but absent with the Horn and Yeh connectomes. As such, those basal ganglia pathways represent examples of false negative results for the tractography-based connectomes.

Visual inspection of the VC DBS results shows some general consistencies across connectomes. They all show activation of projections anteriorly to the ventral pre-frontal cortex, as well as posteriorly into the brainstem. The Horn and Yeh connectomes also highlight activation of projections into the occipital and temporal lobes, primarily via streamlines associated with the anterior commissure. In contrast, construction of the Petersen connectome did not account for the anterior commissure, and hence represent examples of false negative results for that connectome.

Visual inspection of the ANT DBS results also show some general consistencies across connectomes with common predictions of anteriorly projecting streamlines into the prefrontal cortex, as well as activation of the fornix. The Horn and Majtanik connectomes both show some activation of the inferior thalamic peduncle and connectivity with the temporal lobe, but these projections are lacking in the Yeh connectome. One area of discrepancy is the prominent activation of projections to cingulate cortex in the Majtanik

connectome, which are lacking in both the Horn and Yeh connectomes. This pathway likely represents a false negative result for the tractography-based connectomes.

Visual inspection of the VIM DBS results reveal some similarities across connectomes, with all showing an activation of projections posteriorly to the cerebellum. Additionally, both the Horn and Yeh connectomes show common predictions of activation dorsally to the motor cortex, as well as into the brainstem. However, the tractography connectomes consist of activated streamlines that run continuously from motor cortex, through the thalamus, and into the cerebellum. Anatomically, these streamlines are actually two separate pathways, consisting of the cerebellothalamic and thalamocortical projections, respectively. As such, the Petersen connectome shows no direct cortical activation with VIM DBS because it does not have representation of the thalamocortical pathway.

3.2. Patterns of DBS cortical connectivity

To better characterize pathway activation variability across the connectomes, we constructed activation-dependent cortical connectivity profiles from each DBS target location. The connectivity profiles were estimated by first parcellating the CIT168 brain into 34 cortical ROIs (Fig. 4, supplementary Fig. S1), and then calculating the distribution of activated streamlines terminating at each ROI. We then used profile-plots to represent the proportion of activated streamlines that project to the indicated ROI, across the different DBS targets (Fig. 4, supplementary Fig. S4). The connectivity profiles reveal low agreement across the connectomes, in terms of their predictions of which cortical territories are connected to a DBS target. Even for cases when the connectomes predicted a DBS target projecting to the same ROIs, the distribution of representative streamlines across these ROIs was substantially different (Fig. 4, supplementary Fig. S4).

For STN DBS, the connectivity pattern of the Petersen connectome was notably different than the tractography-based connectomes (Fig. 4). For example, the activated streamlines of the Petersen connectome were more uniformly spread across motor cortical regions, while the Yeh (83.9 %) and Horn (84.0 %) connectomes primarily connected to the superior frontal gyrus. However, the most striking result was that for a given activation sphere of 3 mm, the Yeh connectome had 0 %, and the Horn connectome had only 4.8 % of its activated streamlines connecting to the primary motor (precentral) region in the brain. In comparison, the Petersen connectome had about 34.0 % of its activated streamlines projecting to the precentral ROI.

For VC DBS, the Horn connectome projected to a substantially greater number (16) of ROIs than either the Yeh (8) or Petersen (5) connectomes (Fig. 4). The Petersen and Yeh connectomes projected predominantly to the medial orbitofrontal (92.7 %) and lateral occipital (59.8 %) regions, respectively. Alternatively, the Horn connectome had streamlines widely dispersed across all of its connecting ROIs.

For ANT DBS, while all connectomes had streamlines projecting to the prefrontal cortex, they varied in the proportion of streamlines distributed across the connecting ROIs (Fig. 4). The Yeh connectome projected primarily to rostral middle frontal (51 %), the Horn connectome to pars orbitalis (37 %) and superior frontal (32 %), while the Majtanik

connectome to rostral middle frontal (39 %) and lateral orbital frontal (28 %). Also, while the Yeh and Horn connectomes had almost no streamlines projecting to medially located regions in the brain, the Majtanik connectome had medial connections to the frontal pole (11 %), medial orbital frontal (5 %), and caudal anterior cingulate (5 %).

For VIM DBS, the Petersen connectome had no streamlines projecting to the cortex for the given activation sphere of 3 mm, due to its lack of thalamocortical pathways (Fig. 3). Both the Horn and Yeh connectomes had an overwhelming majority of streamlines (> 92 %) projecting to the superior frontal and precentral gyrus, however, the proportion of streamlines distributed across these two ROIs was inversely distributed within each connectome (supplementary Fig. S4). Specifically, the Horn connectome projected predominantly to superior frontal (61 %), while the Yeh connectome projected predominantly to precentral (67 %).

3.3. Quantifying variability in DBS connectivity

To quantify and compare pathway activation variability across different atlases, we calculated the Dice overlap coefficients and bundle adjacency scores at each target location (Fig. 5). The median Dice overlap coefficients were largely in the range of 0.1 and 0.2 for all DBS targets, indicating very low agreement between the activated streamlines of the different connectomes. As a voxel based measure, Dice overlap is sensitive to the spatial spread and number of activated streamlines in each set. Consistent with this fact, the Dice overlap coefficients between the wide-ranging normative connectome and the region-focused histology-based connectomes were the lowest (and also had the least interquartile spread) across all three target locations. The volume similarity between the Majtanik and Yeh connectomes was the highest among all compared pairs, with a median Dice overlap of 0.28 for ANT DBS.

The median bundle adjacency scores were <0.65 for all DBS targets, indicating low to moderate agreement in the shape of activated streamlines between connectomes (Fig. 5). The bundle adjacency score can intuitively be interpreted as the likelihood that the streamlines within the two sets being compared are samples from a common superset. For example, the Petersen and Yeh connectomes were completely dissimilar in shape, with a median bundle adjacency of <0.02 for the STN, VC, and VIM targets. In comparison, while also being histology-based, the Majtanik connectome showed much higher similarity to Yeh, with a median bundle adjacency of 0.37 for ANT DBS. The bundle adjacency metric also favored the high spatial spread and number of activated streamlines in the Horn normative connectome (which was penalized by the Dice coefficient analyses), as observed by the relatively higher scores involving the Horn connectome. The Horn and Yeh connectome had the highest median bundle adjacency among all compared pairs (0.65 for VIM DBS and 0.49 for VC DBS).

We used the Jensen-Shannon distance (JSD) to quantify the divergence between the activation-dependent connectivity profiles of different connectomes (Fig. 6). Given an activation sphere radius, and target location, JSD was calculated pairwise between the connectivity profile distribution of each connectome (Fig. 6a). For easier interpretability we report the 1-JSD value and refer to it as the Jensen Shannon similarity (JSS) score.

The connectivity profile distributions were also found to be significantly different, $p < 0.001$ for all pairs compared, estimated using the two-tailed Fishers exact test. With two exceptions, the median JSS scores were <0.3 for all DBS targets, indicating significant variability in the cortical distribution of streamlines across connectomes. The exceptions were the scores between Horn and Yeh connectomes for STN DBS (median JSS of 0.45) and VIM DBS (median JSS of 0.42). Notably, each of these exception cases was characterized by a skewed distribution in which the overwhelming majority of streamlines (>84 %) in both connectomes projected to just one or two ROIs (Fig. 6a, supplementary Fig. S4). VC DBS exhibited the overall lowest JSS across all targets, especially between the Petersen and Yeh connectomes (median JSS of 0.01), indicating that streamlines in these connectomes projected to exclusively different cortical ROIs.

We used the weighted degree centrality (WDC) metric as a summary statistic to quantify the overall cortical connectivity of a DBS target for a given connectome (Fig. 6). A higher WDC score indicates a dense network of activated streamlines spread across several cortical ROIs, while a low WDC score indicates sparse and/or heterogeneous DBS connectivity (i.e., just a few ROIs account for a majority of the streamlines). It is important to note however, that WDC solely measures connection strength and reveals no information regarding the anatomical accuracy of the connection. The WDC measure is therefore susceptible to being impacted by false-positive connections which can inflate WDC, or under-representation of actual pathways (i.e. false-negative connections) which can lower WDC. In theory, an ideal connectomic resource would have a high WDC score across all target locations, while also being anatomically accurate (shown as a green triangular region in Fig. 6c).

VC DBS in the Horn connectome exhibited the highest WDC score (8.4 ± 4.6) across all connectomes and target locations. However, unannotated whole brain connectomes are known to contain a high number of false-positive connections (Maier-Hein et al., 2017), and our example results with STN DBS and ANT DBS also highlight the false-positive nature of the Horn connectome (Fig. 2). Other high WDC scores included STN DBS (3.7 ± 1.8) for the Petersen connectome and ANT DBS (4.0 ± 2.0) for the Majtanik connectome, consistent with the fact that the pathways in the Petersen and Majtanik connectome were explicitly designed for the subthalamic region and the anterior thalamic region, respectively. Both the Yeh and Horn connectomes had noticeably lower WDC scores for STN DBS, indicating an under-representation of pathways to ROIs other than prefrontal cortex (Fig. 4). VIM DBS exhibited the lowest overall scores (mean WDC < 2.0) indicating localized cortical connectivity to the sensorimotor areas in the Horn and Yeh connectomes, and the lack of thalamocortical pathway representation in the Petersen connectome. Interestingly, ANT DBS scores for the Yeh and Horn connectomes were nearly identical, since WDC only factors in the connection weights and not the specific ROIs to which the DBS target is actually connected (see supplementary Fig. S4).

4. Discussion

The structural connectome is the fundamental base of most connectomic DBS modeling analyses. However, side-by-side comparison of the predicted DBS pathway activation showed that results can vary substantially depending on the choice of connectome used

in the analysis. While each connectome has its own strengths and weaknesses, they each resulted in differing connectivity profiles for identical DBS conditions in four common DBS targets. The activated streamlines projected to notably different areas of the brain in each case. Quantitative analysis indicates significant variability in the volume (median Dice overlap < 0.3), shape (median bundle adjacency < 0.65), and cortical distribution (median JSS < 0.45, $p < 0.001$) of streamlines between connectomes. This variability can lead to inconsistent and potentially erroneous inferences of DBS target connectivity, even when all other sources of variation such as electrode localization, activation model, and patient-specific factors are eliminated. Given that these inconsistencies stem from the connectome, the general validity of "connectomic DBS" analyses must be questioned unless there has been stringent anatomical and/or electrophysiological validation of the underlying connectome model used in a given study.

The aim of this study is not to detract from the potential scientific utility of connectomic atlases, but instead highlight that connectomic DBS is a relatively new subfield of research whose rapid growth in clinical popularity has outpaced the necessary steps of rigorous validation for its modeling components. This unfortunate fact has been consistently noted for many years, first at the DBS electric field level (Chaturvedi et al., 2010), then at the pathway activation level (Gunalan et al., 2018), and here at the connectome level (Fig. 4). Consequently, inferences derived from connectomic DBS studies often exhibit a degree of optimism that exceeds what the biophysical modeling strategy and underlying connectomic data can robustly substantiate (e.g. Hollunder et al., 2024; Li et al., 2020). Alternatively, the results of this study suggest that the field of connectomic DBS needs to take a step back and first focus on identifying and/or developing anatomically validated structural connectomes for specific brain targets of interest. Such tools are beginning to become available for the STN (Petersen et al., 2019), ANT (Majtanik et al., 2022), and brainstem (Adil et al., 2021). In addition, major investments from the NIH BRAIN CONNECTS program are providing the scientific foundations to facilitate creation of many more histology-based pathway atlases in the human brain.

The few studies (Hollunder et al., 2024; Li et al., 2020) that have previously investigated connectome bias in DBS analyses have done so in the limited context of comparing the connectome's ability to correlate with clinical outcomes. For instance, Li et al. (2020) repeated their OCD DBS analysis using a normative connectome constructed from 985 HCP subjects, as well as the Petersen connectome. They identified streamlines within both connectomes that showed similar correlation scores (R-values) to positive patient outcome, but for completely different pathways. The normative connectome predicted primary connectivity to the ventrolateral and medial prefrontal cortex, while the Petersen connectome predicted primary connectivity to the dorsal anterior cingulate cortex (dACC). A similar approach was employed by Hollunder et al. (2024) for STN DBS where they analyzed four connectomes, including the 985 HCP normative connectome, Petersen connectome, an amended Yeh connectome, and a patient-specific connectome. However, the authors largely overlooked the differing cortical connectivity exhibited by each connectome (Fig. 4), and instead focused on the similar R-values that each connectome showed with respect to explaining variance in clinical outcomes. However, the ability of a connectome to predict clinical outcome is not an indicator of its anatomical accuracy (Dembek et al.,

2022), and nor are similar correlation scores for connectomes an indicator of similar DBS connectivity.

Our analyses suggest that the noble goal of creating a single whole brain connectome from HCP datasets (e.g. Yeh, 2022), and then using it in DBS research appears to be somewhat premature (Coenen et al., 2019). This is because the best approach for estimating and annotating pathway trajectories in the human brain remains a daunting challenge from DWI data alone (Maier-Hein et al., 2017; Schilling et al., 2021). The variability arising from just the choice of bundle-segmentation protocol alone can be greater than the variability due to either acquisition, registration, or patient-specific variability (Schilling et al., 2021). For example, our results show that the streamline variability due to the choice of connectome (i.e. median volume Dice overlap < 0.3 (Fig. 5)) matches the DWI protocol variability results reported in Schilling et al. (2021). Given the lack of standardization in tractography, combined with the connectomic DBS prediction variability exhibited in this study, there remains a critical need to first rigorously validate if *in silico* computational models of brain connectivity actually provide a reliable surrogate for in vivo brain anatomy (Yendiki et al., 2022).

One potential way to bridge this gap between *in silico* and *in vivo* is to first use anatomically realistic connectomes and then evaluate the accuracy of the model-based DBS predictions by using cortical evoked responses as a biomarker of pathway activation (Adkinson et al., 2022; Howell et al., 2021; Schmidt et al., 2020; Seas et al., 2024). For example, electrocorticography (ECoG) confirmation of the motor hyperdirect pathway (HDP) activation during STN DBS has been reported by Miocinovic et al. (2018). Those authors found the presence of evoked potentials to be the highest in the primary motor (M1) and premotor areas, and that the amplitude of the M1 potential was predictive of the final therapeutic stimulation contact used for the patient. In contrast, *in silico* studies employing normative connectomes for investigating STN DBS in patients with PD, have primarily reported a positive therapeutic effect from the activation of STN to premotor pathways, but importantly a (null) or negative effect from the activation of STN to M1 pathways (Hollunder et al., 2024; Wang et al., 2021). The likely reason for this contrarian *in silico* result is the strong anterior projection bias in the tractography-based (Yeh and Horn) connectomes for STN DBS (Figs. 2, 4), and the lack of an anatomically defined hyperdirect pathway that accurately captures the M1 to STN connectivity (Petersen et al., 2019). Alternatively, ECoG potentials recorded during STN DBS have been used to validate the motor HDP and corticospinal/bulbar pathway activations predicted by DBS modeling with the Petersen connectome (Howell et al., 2021).

Stereo-electroencephalographic (sEEG) recordings have also been used to evaluate the predicted DBS connectivity for VC DBS with patient-specific probabilistic tractography (Adkinson et al., 2022). The regions that registered the most prominent evoked potentials were the ventral (both ventrolateral and ventromedial) prefrontal cortex (vPFC), medial orbitofrontal cortex (mOFC), and the anterior cingulate cortex (ACC). Despite growing evidence towards ACC involvement in VC DBS, *in silico* modeling using normative connectomes (Baldermann et al., 2021; Li et al., 2020), as well as patient-specific tractography (Adkinson et al., 2022; Widge et al., 2021), have yet to adequately isolate

VC pathways linking to ACC. However, this track is defined in the histology-based Petersen connectome (Petersen et al., 2019) and its activation was correlated with thereapeutic benefit in supplemental analyses by Li et al. (2020). Further, while several studies have implicated the importance of pathways connecting vPFC as important to OCD response (Baldermann et al., 2021; Mosley et al., 2021), there remains ambiguity on whether the activation of these pathways have a positive or negative association to therapeutic outcome (Widge et al., 2021). Our results partially illuminate these underlying structural inconsistencies, with VC DBS eliciting significant differences between connectomes in their distribution of representative streamlines to each of the aforementioned regions, vPFC, mOFC and ACC (Fig. 4). In fact, out of the three DBS targets analyzed, VC DBS had by far the highest variability in cortical connectivity across connectomes, with a median JSS < 0.12 (Fig. 6).

Several recent studies have implicated the cerebellothalamic tract (CBT, also referred to as the dentatorubrothalamic tract) as a key modulation target for effective tremor reduction in VIM DBS (Brinda et al., 2023; Coenen et al., 2020; Middlebrooks et al., 2022). However, accurate tractographic reconstruction of the decussating fibers in the CBT remains a challenge, as does the connectivity profile mapping of the thalamocortical pathways associated with the VIM, especially in clinical DWI datasets with poor signal-to-noise ratio. Therefore, experimental analyses are needed to better understand the network effects of VIM DBS. Magnetoencephalography (MEG) experiments (Hartmann et al., 2018) have demonstrated that the cortical responses evoked during VIM DBS are predominantly localized to the primary motor (M1) and somatosensory (S1) cortex. However, a recent ECoG study (Conner et al., 2024) found no early response in the M1 at normal clinical DBS ranges for direct CBT stimulation. As such, that study did not support the connectomic DBS predictions of direct axonal connections from the stimulation site to M1, suggesting that M1 modulation by VIM DBS was the result of intermediary connections (most likely through synapses in the VIM). Meanwhile, connectomic DBS modeling studies (using patient-specific, as well as normative data) have been widely used in attempts to identify cortical areas that are associated with effective clinical targeting in VIM DBS. Some studies (Middlebrooks et al., 2018, 2021) have identified connectivity with pre-motor / supplementary motor areas as significant predictor for effective tremor suppression, while other similar analyses (Akram et al., 2018; Al-Fatly et al., 2019; Grimm et al., 2025) have identified connectivity to M1 and S1 as being more relevant to clinical outcome. These inconsistencies can be at least partially explained with our analyses (Fig. 4), and the role of connectome selection on the simulated results. For example, while both the Horn and Yeh connectomes projected predominantly to the sensorimotor cortices (mean WDC < 2.0) with VIM DBS, they varied substantially in their distribution of streamlines across the superior frontal (parts of the SMA) and precentral (M1) gyrus (Fig. 4).

Accurate structural connectomic modeling for ANT DBS also remains an ongoing challenge (Grodd et al., 2020; Majtanik et al., 2022). One major reason being the variability and complexity of the possible pathways implicated in the epileptogenic network (Middlebrooks et al., 2020; Osorio et al., 2021). These include the mammillothalamic and the thalamocingulate tracts (Schaper et al., 2020; Weininger et al., 2019), which were synthetically reconstructed in the Majtanik connectome (Fig. 3), but are typically absent in population-averaged tractography connectomes, including the Horn and Yeh connectomes.

So far, electrophysiological validation analyses remain to be attempted for connectomic ANT DBS models, or almost any other DBS target in the brain. Nonetheless, despite the technical and logistic challenges of measuring intracranial electrophysiology during DBS, these recordings provide a much needed benchmark to help verify if connectomic DBS modeling predictions have any legitimacy.

4.1. Limitations

There are several limitations and constraints applicable to the analyses presented in this study. For example, our results provided a side-by-side comparison of the variability across connectomes, but they offer no insight as to whether the predicted pathway activation of one connectome is more accurate than another, or if these connectomes each capture unique partial aspects of the true underling connectivity in the brain. As discussed above, these factors need to be validated by independent anatomical and/or electrophysiological analyses. Unfortunately, the vast majority of connectomic DBS studies published in the clinical literature have failed to perform those validations (Neudorfer et al., 2023), and as such, substantial skepticism is warranted on their conclusions. Some of the other limitations of our study include: 1) the use of a single reference brain that does not necessarily represent the anatomy of an individual subject brain (Pauli et al., 2018); 2) the use of spherical activation volumes that do not incorporate detailed biophysical properties of neural activation such as fiber diameters, tissue anisotropy, or polarity configurations (Howell et al., 2019); 3) the relatively small sample size of four connectomes and four DBS target regions; and 4) the derived cortical connectivity estimates depend on the ROI parcellation scheme. In addition, no single measure can capture all dimensions of variability in a complex network. Instead, we employed a combination of similarity (Dice, bundle adjacency), information-theoretic (JSD), and network analysis (WDC) metrics to capture different aspects of heterogeneity in network connections.

4.2. Conclusion

There is no denying the potential scientific utility, or clinical excitement, associated with connectomic DBS analyses, and they are poised to provide many important insights into the network effects of DBS therapy. However, the technical details of the model systems need to be properly vetted to meet the scientific demands of the desired analyses. Unfortunately, the connectomic DBS literature has prematurely relied on connectomes that lack independent anatomical and/or electrophysiological validation. As such, identical DBS simulations with different connectomes generate highly inconsistent results. These issues substantially reduce confidence in a generally promising DBS research strategy. In turn, there appears to be much work remaining in the creation of accurate human connectomes for DBS research.

Supplementary Material

Refer to Web version on PubMed Central for supplementary material.

Acknowledgements

This work was supported by grants from the National Institutes of Health (R37 NS116079; UM1 NS132358). The authors thank Milan Majtanik and MRX-Brain for providing access to the ANT connectome.

Data and code availability statement

Data and code used to generate the results presented in this study are available for download in the Open Science Framework (https://osf.io/byhgk/). This includes VTK formatted streamline datasets associated with the Horn, Yeh, and Petersen connectomes, registered to a common CIT168 space. The Majtanik pathway atlas is not publicly available, but is available from its original authors upon reasonable request (Majtanik et al., 2022).

References

Adil SM, Calabrese E, Charalambous LT, Cook JJ, Rahimpour S, Atik AF, Cofer GP, Parente BA, Johnson GA, White LE, 2021. A high-resolution interactive atlas of the human brainstem using magnetic resonance imaging. Neuroimage 237, 118135. 10.1016/j.neuroimage.2021.118135. [PubMed: 33951517]

Adkinson JA, Tsolaki E, Sheth SA, Metzger BA, Robinson ME, Oswalt D, McIntyre CC, Mathura RK, Waters AC, Bijanki KR, 2022. Imaging versus electrographic connectivity in human mood-related fronto-temporal networks. Brain Stimul. 15 (3), 554–565. 10.1016/j.brs.2022.03.002. [PubMed: 35292403]

Akram H, Dayal V, Mahlknecht P, Georgiev D, Hyam J, Foltynie T, Limousin P, De Vita E, Jahanshahi M, Zrinzo L, 2018. Connectivity derived thalamic segmentation in deep brain stimulation for tremor. NeuroImage: Clinical 18, 130–142. 10.1016/j.nicl.2018.01.008. [PubMed: 29387530]

Akram H, Sotiropoulos SN, Jbabdi S, Georgiev D, Mahlknecht P, Hyam J, Foltynie T, Limousin P, De Vita E, Zrinzo L, 2017. Subthalamic deep brain stimulation sweet spots and hyperdirect cortical connectivity in Parkinson's disease. Neuroimage 158, 332–345. 10.1016/j.neuroimage.2017.07.012. [PubMed: 28711737]

Al-Fatly B, Ewert S, Kübler D, Kroneberg D, Horn A, Kühn AA, 2019. Connectivity profile of thalamic deep brain stimulation to effectively treat essential tremor. Brain 142 (10), 3086–3098. 10.1093/brain/awz236. [PubMed: 31377766]

Archer DB, Vaillancourt DE, Coombes SA, 2018. A Template and Probabilistic Atlas of the Human Sensorimotor Tracts using Diffusion MRI. Cerebral Cortex 28 (5), 1685–1699. 10.1093/cercor/bhx066. [PubMed: 28334314]

Avants BB, Tustison NJ, Song G, Cook PA, Klein A, Gee JC, 2011. A reproducible evaluation of ANTs similarity metric performance in brain image registration. Neuroimage 54 (3), 2033–2044. 10.1016/j.neuroimage.2010.09.025. [PubMed: 20851191]

Baldermann JC, Schüller T, Kohl S, Voon V, Li N, Hollunder B, Figee M, Haber SN, Sheth SA, Horn A, 2021. Connectomic Deep Brain Stimulation for Obsessive-Compulsive Disorder. Biol. Psychiatry 90 (10), 678–688. 10.1016/j.biopsych.2021.07.010. [PubMed: 34482949]

Bower KL, Noecker AM, Frankemolle-Gilbert AM, McIntyre CC, 2023. Model-Based Analysis of Pathway Recruitment During Subthalamic Deep Brain Stimulation. Neuromodulation. 10.1016/j.neurom.2023.02.084.

Brinda A, Slopsema JP, Butler RD, Ikramuddin S, Beall T, Guo W, Chu C, Patriat R, Braun H, Johnson MD, 2023. Lateral cerebellothalamic tract activation underlies DBS therapy for Essential Tremor. Brain Stimul. 16 (2), 445–455. 10.1016/j.brs.2023.02.002. [PubMed: 36746367]

Butson CR, McIntyre CC, 2006. Role of electrode design on the volume of tissue activated during deep brain stimulation. J. Neural Eng 3 (1), 1–8. 10.1088/1741-2560/3/1/001. [PubMed: 16510937]

Candeloro L, Savini L, Conte A, 2016. A New Weighted Degree Centrality Measure: The Application in an Animal Disease Epidemic. PLoS. One 11 (11), e0165781. 10.1371/journal.pone.0165781. [PubMed: 27802327]

Chandio BQ, Risacher SL, Pestilli F, Bullock D, Yeh FC, Koudoro S, Rokem A, Harezlak J, Garyfallidis E, 2020. Bundle analytics, a computational framework for investigating the shapes and profiles of brain pathways across populations. Sci. Rep 10, 17149. 10.1038/s41598-020-74054-4. [PubMed: 33051471]

Chaturvedi A, Butson CR, Lempka SF, Cooper SE, McIntyre CC, 2010. Patient-specific models of deep brain stimulation: Influence of field model complexity on neural activation predictions. Brain Stimul. 3 (2), 65–77. 10.1016/j.brs.2010.01.003. [PubMed: 20607090]

Coenen VA, Sajonz B, Prokop T, Reisert M, Piroth T, Urbach H, Jenkner C, Reinacher PC, 2020. The dentato-rubro-thalamic tract as the potential common deep brain stimulation target for tremor of various origin: An observational case series. Acta Neurochir. (Wien) 162 (5), 1053–1066. 10.1007/s00701-020-04248-2. [PubMed: 31997069]

Coenen VA, Schlaepfer TE, Varkuti B, Schuurman PR, Reinacher PC, Voges J, Zrinzo L, Blomstedt P, Fenoy AJ, Hariz M, 2019. Surgical decision making for deep brain stimulation should not be based on aggregated normative data mining. Brain Stimul. 12 (6), 1345–1348. 10.1016/j.brs.2019.07.014. [PubMed: 31353286]

Conner CR, Forseth KJ, Lozano AM, Ritter R, Fenoy AJ, 2024. Thalamo-cortical evoked potentials during stimulation of the dentato-rubro-thalamic tract demonstrate synaptic filtering. Neurotherapeutics. 21 (1), e00295. 10.1016/j.neurot.2023.10.005. [PubMed: 38237402]

Dembek TA, Baldermann JC, Petry-Schmelzer JN, Jergas H, Treuer H, Visser-Vandewalle V, Dafsari HS, Barbe MT, 2022. Sweetspot Mapping in Deep Brain Stimulation: Strengths and Limitations of Current Approaches. Neuromodulation. 25 (6), 877–887. 10.1111/ner.13356. [PubMed: 33476474]

Desikan RS, Ségonne F, Fischl B, Quinn BT, Dickerson BC, Blacker D, Buckner RL, Dale AM, Maguire RP, Killiany RJ, 2006. An automated labeling system for subdividing the human cerebral cortex on MRI scans into gyral based regions of interest. Neuroimage 31 (3), 968–980. 10.1016/j.neuroimage.2006.01.021. [PubMed: 16530430]

Dice LR, 1945. Measures of the Amount of Ecologic Association Between Species. Ecology. 26 (3), 297–302. 10.2307/1932409.

Elias GJB, Germann J, Loh A, Boutet A, Taha A, Wong EHY, Parmar R, Lozano AM, 2022. Chapter 12—Normative connectomes and their use in DBS. In: Horn A (Ed.), Connectomic Deep Brain Stimulation. Academic Press, pp. 245–274. 10.1016/B978-0-12-821861-7.00014-2.

Endres DM, Schindelin JE, 2003. A new metric for probability distributions. IEEe Trans. Inf. Theory 49 (7), 1858–1860. 10.1109/TIT.2003.813506.

Fischl B, 2012. FreeSurfer. Neuroimage 62 (2), 774–781. 10.1016/j.neuroimage.2012.01.021. [PubMed: 22248573]

Fisher R, Salanova V, Witt T, Worth R, Henry T, Gross R, Oommen K, Osorio I, Nazzaro J, SANTE Study Group, 2010. Electrical stimulation of the anterior nucleus of thalamus for treatment of refractory epilepsy. Epilepsia 51 (5), 899–908. 10.1111/j.1528-1167.2010.02536.x. [PubMed: 20331461]

Garyfallidis E, Brett M, Amirbekian B, Rokem A, Van Der Walt S, Descoteaux M, Nimmo-Smith I, 2014. Dipy, a library for the analysis of diffusion MRI data. Front. Neuroinform 8. 10.3389/fninf.2014.00008. [PubMed: 24600385]

Garyfallidis E, Brett M, Correia MM, Williams GB, Nimmo-Smith I, 2012. QuickBundles, a Method for Tractography Simplification. Front. Neurosci 6. 10.3389/fnins.2012.00175. [PubMed: 22347152]

Grimm F, Walcker M, Milosevic L, Naros G, Bender B, Weiss D, Gharabaghi A, 2025. Strong connectivity to the sensorimotor cortex predicts clinical effectiveness of thalamic deep brain stimulation in essential tremor. NeuroImage: Clinical 45, 103709. 10.1016/j.nicl.2024.103709. [PubMed: 39608226]

Grodd W, Kumar VJ, Schüz A, Lindig T, Scheffler K, 2020. The anterior and medial thalamic nuclei and the human limbic system: Tracing the structural connectivity using diffusion-weighted imaging. Sci. Rep 10 (1), 10957. 10.1038/s41598-020-67770-4. [PubMed: 32616764]

Gunalan K, Howell B, McIntyre CC, 2018. Quantifying axonal responses in patient-specific models of subthalamic deep brain stimulation. Neuroimage 172, 263–277. 10.1016/j.neuroimage.2018.01.015. [PubMed: 29331449]

Hartmann CJ, Hirschmann J, Vesper J, Wojtecki L, Butz M, Schnitzler A, 2018. Distinct cortical responses evoked by electrical stimulation of the thalamic ventral intermediate nucleus and of the subthalamic nucleus. NeuroImage: Clinical 20, 1246–1254. 10.1016/j.nicl.2018.11.001. [PubMed: 30420259]

Hines K, Noecker AM, Frankemolle-Gilbert AM, Liang TW, Ratliff J, Heiry M, McIntyre CC, Wu C, 2024. Prospective Connectomic-Based Deep Brain Stimulation Programming for Parkinson's Disease. Mov. Disord 39 (12), 2249–2258. 10.1002/mds.30026. [PubMed: 39431498]

Hitti FL, Widge AS, Riva-Posse P, Malone DA, Okun MS, Shanechi MM, Foote KD, Lisanby SH, Ankudowich E, Pouratian N, 2023. Future directions in psychiatric neurosurgery: Proceedings of the 2022 American Society for Stereotactic and Functional Neurosurgery meeting on surgical neuromodulation for psychiatric disorders. Brain Stimul. 16 (3), 867–878. 10.1016/j.brs.2023.05.011. [PubMed: 37217075]

Hollunder B, Ostrem JL, Sahin IA, Rajamani N, Oxenford S, Butenko K, Neudorfer C, Reinhardt P, Zvarova P, Horn A, 2024. Mapping dysfunctional circuits in the frontal cortex using deep brain stimulation. Nat. Neurosci 27 (3), 573–586. 10.1038/s41593-024-01570-1. [PubMed: 38388734]

Horn A, Reich M, Vorwerk J, Li N, Wenzel G, Fang Q, Schmitz-Hübsch T, Nickl R, Kupsch A, Volkmann J, Kühn AA, Fox MD, 2017. Connectivity Predicts deep brain stimulation outcome in Parkinson disease. Ann. Neurol 82 (1), 67–78. 10.1002/ana.24974. [PubMed: 28586141]

Howell B, Gunalan K, McIntyre CC, 2019. A Driving-Force Predictor for Estimating Pathway Activation in Patient-Specific Models of Deep Brain Stimulation. Neuromodulation. 22 (4), 403–415. 10.1111/ner.12929. [PubMed: 30775834]

Howell B, Isbaine F, Willie JT, Opri E, Gross RE, Hemptinne CD, Starr PA, McIntyre CC, Miocinovic S, 2021. Image-based biophysical modeling predicts cortical potentials evoked with subthalamic deep brain stimulation. Brain Stimul. 14 (3), 549–563. 10.1016/j.brs.2021.03.009. [PubMed: 33757931]

Krack P, Volkmann J, Tinkhauser G, Deuschl G, 2019. Deep Brain Stimulation in Movement Disorders: From Experimental Surgery to Evidence-Based Therapy. Movement Disorders 34 (12), 1795–1810. 10.1002/mds.27860. [PubMed: 31580535]

Li N, Baldermann JC, Kibleur A, Treu S, Akram H, Elias GJB, Boutet A, Lozano AM, Al-Fatly B, Horn A, 2020. A unified connectomic target for deep brain stimulation in obsessive-compulsive disorder. Nat. Commun 11 (1), Article 1. 10.1038/s41467-020-16734-3.

Lin J, 1991. Divergence measures based on the Shannon entropy. IEEe Trans. Inf. Theory 37 (1), 145–151. 10.1109/18.61115. IEEE Transactions on Information Theory.

Lujan JL, Chaturvedi A, Malone DA, Rezai AR, Machado AG, McIntyre CC, 2012. Axonal pathways linked to therapeutic and nontherapeutic outcomes during psychiatric deep brain stimulation. Hum. Brain Mapp 33 (4), 958–968. 10.1002/hbm.21262. [PubMed: 21520343]

Maier-Hein KH, Neher PF, Houde JC, Côté MA, Garyfallidis E, Zhong J, Chamberland M, Yeh FC, Lin YC, Descoteaux M, 2017. The challenge of mapping the human connectome based on diffusion tractography. Nat. Commun 8 (1), 1349. 10.1038/s41467-017-01285-x. [PubMed: 29116093]

Majtanik M, Gielen F, Coenen VA, Lehtimäki K, Mai JK, 2022. Structural connectivity of the ANT region based on human ex-vivo and HCP data. Relevance for DBS in ANT for epilepsy. Neuroimage 262, 119551. 10.1016/j.neuroimage.2022.119551. [PubMed: 35948264]

Middlebrooks EH, Domingo RA, Vivas-Buitrago T, Okromelidze L, Tsuboi T, Wong JK, Eisinger RS, Almeida L, Burns MR, Grewal SS, 2020. Neuroimaging Advances in Deep Brain Stimulation: Review of Indications, Anatomy, and Brain Connectomics. American Journal of Neuroradiology 41 (9), 1558–1568. 10.3174/ajnr.A6693. [PubMed: 32816768]

Middlebrooks EH, Okromelidze L, Carter RE, Jain A, Lin C, Westerhold E, Peña AB, Quiñones-Hinojosa A, Uitti RJ, Grewal SS, 2022. Directed stimulation of the dentato-rubro-thalamic tract for deep brain stimulation in essential tremor: a blinded clinical trial. Neuroradiol. J 35 (2), 203–212. 10.1177/19714009211036689. [PubMed: 34340623]

Middlebrooks EH, Okromelidze L, Wong JK, Eisinger RS, Burns MR, Jain A, Lin HP, Yu J, Opri E, Tsuboi T, 2021. Connectivity correlates to predict essential tremor deep brain stimulation outcome: Evidence for a common treatment pathway. NeuroImage: Clinical 32, 102846. 10.1016/j.nicl.2021.102846. [PubMed: 34624639]

Middlebrooks EH, Tuna IS, Almeida L, Grewal SS, Wong J, Heckman MG, Lesser ER, Bredel M, Foote KD, Holanda VM, 2018. Structural connectivity–based segmentation of the thalamus and prediction of tremor improvement following thalamic deep brain stimulation of the ventral

intermediate nucleus. NeuroImage: Clinical 20, 1266–1273. 10.1016/j.nicl.2018.10.009. [PubMed: 30318403]

Miocinovic S, Hemptinne C.de, Chen W, Isbaine F, Willie JT, Ostrem JL, Starr PA, 2018. Cortical Potentials Evoked by Subthalamic Stimulation Demonstrate a Short Latency Hyperdirect Pathway in Humans. Journal of Neuroscience 38 (43), 9129–9141. 10.1523/JNEUROSCI.1327-18.2018. [PubMed: 30201770]

Mosley PE, Windels F, Morris J, Coyne T, Marsh R, Giorni A, Mohan A, Sachdev P, O'Leary E, Silburn PA, 2021. A randomised, double-blind, sham-controlled trial of deep brain stimulation of the bed nucleus of the stria terminalis for treatment-resistant obsessive-compulsive disorder. Transl. Psychiatry 11 (1), 1–17. 10.1038/s41398-021-01307-9. [PubMed: 33414379]

Neudorfer C, Butenko K, Oxenford S, Rajamani N, Achtzehn J, Goede L, Hollunder B, Ríos AS, Hart L, Horn A, 2023. Lead-DBS v3.0: Mapping deep brain stimulation effects to local anatomy and global networks. Neuroimage 268, 119862. 10.1016/j.neuroimage.2023.119862. [PubMed: 36610682]

Nielsen F, 2019. On the Jensen–Shannon Symmetrization of Distances Relying on Abstract Means. Entropy 21 (5), 485. 10.3390/e21050485. [PubMed: 33267199]

Noecker AM, Choi KS, Riva-Posse P, Gross RE, Mayberg HS, McIntyre CC, 2018. StimVision Software: Examples and Applications in Subcallosal Cingulate Deep Brain Stimulation for Depression. Neuromodulation. 21 (2), 191–196. 10.1111/ner.12625. [PubMed: 28653482]

Noecker AM, Frankemolle-Gilbert AM, Howell B, Petersen MV, Beylergil SB, Shaikh AG, McIntyre CC, 2021. StimVision v2: Examples and Applications in Subthalamic Deep Brain Stimulation for Parkinson's Disease. Neuromodulation. 24 (2), 248–258. 10.1111/ner.13350. [PubMed: 33389779]

Osorio I, Giftakis J, Stypulkowski P, Tonder L, 2021. Anatomical connectivity and efficacy of electro-therapy for seizure control: a SANTE's single-center regression analyses. Epilepsy & Behavior 115. 10.1016/j.yebeh.2020.107709.

Pauli WM, Nili AN, Tyszka JM, 2018 A high-resolution probabilistic in vivo atlas of human subcortical brain nuclei. Sci. Data 5 (1), Article 1. 10.1038/sdata.2018.63.

Petersen MV, McIntyre CC, 2023. Comparison of Anatomical Pathway Models with Tractography Estimates of the Pallidothalamic, Cerebellothalamic, and Corticospinal Tracts. Brain Connect. 13 (4), 237–246. 10.1089/brain.2022.0068. [PubMed: 36772800]

Petersen MV, Mlakar J, Haber SN, Parent M, Smith Y, Strick PL, Griswold MA, McIntyre CC, 2019. Holographic Reconstruction of Axonal Pathways in the Human Brain. Neuron 104 (6), 1056–1064. 10.1016/j.neuron.2019.09.030e3. [PubMed: 31708306]

Plantinga BR, Temel Y, Duchin Y, Uludağ K, Patriat R, Roebroeck A, Kuijf M, Jahanshahi A, ter Haar Romenij B, Harel N, 2018. Individualized parcellation of the subthalamic nucleus in patients with Parkinson's disease with 7T MRI. Neuroimage 168, 403–411. 10.1016/j.neuroimage.2016.09.023. [PubMed: 27688203]

Radwan AM, Sunaert S, Schilling K, Descoteaux M, Landman BA, Vandenbulcke M, Theys T, Dupont P, Emsell L, 2022. An atlas of white matter anatomy, its variability, and reproducibility based on constrained spherical deconvolution of diffusion MRI. Neuroimage 254, 119029. 10.1016/j.neuroimage.2022.119029. [PubMed: 35231632]

Rheault F, Benedictis AD, Daducci A, Maffei C, Tax CMW, Romascano D, Caverzasi E, Morency FC, Corrivetti F, Descoteaux M, 2020. Tractostorm: The what, why, and how of tractography dissection reproducibility. Hum. Brain Mapp 41 (7), 1859. 10.1002/hbm.24917. [PubMed: 31925871]

Rosenberg RN, 2015. Circuits and Circuit Disorders: Approaches to Neuromodulation. JAMa Neurol. 72 (11), 1232. 10.1001/jamaneurol.2015.2624. [PubMed: 26409204]

Schaper FLWVJ, Plantinga BR, Colon AJ, Wagner GL, Boon P, Blom N, Gommer ED, Hoogland G, Ackermans L, Temel Y, 2020. Deep Brain Stimulation in Epilepsy: a Role for Modulation of the Mammillothalamic Tract in Seizure Control? Neurosurgery. 87 (3), 602. 10.1093/neuros/nyaa141. [PubMed: 32421806]

Schilling KG, Rheault F, Petit L, Hansen CB, Nath V, Yeh FC, Girard G, Barakovic M, Rafael-Patino J, Descoteaux M, 2021. Tractography dissection variability: What happens when 42

groups dissect 14 white matter bundles on the same dataset? Neuroimage 243, 118502. 10.1016/j.neuroimage.2021.118502. [PubMed: 34433094]

Schmidt SL, Brocker DT, Swan BD, Turner DA, Grill WM, 2020. Evoked Potentials Reveal Neural Circuits Engaged by Human Deep Brain Stimulation. Brain Stimul. 13 (6), 1706–1718. 10.1016/j.brs.2020.09.028. [PubMed: 33035726]

Seas A, Noor MS, Choi KS, Veerakumar A, Obatusin M, Dahill-Fuchel J, Tiruvadi V, Xu E, Riva-Posse P, Howell B, 2024. Subcallosal cingulate deep brain stimulation evokes two distinct cortical responses via differential white matter activation. Proceedings of the National Academy of Sciences 121 (14), e2314918121. 10.1073/pnas.2314918121.

Setsompop K, Kimmlingen R, Eberlein E, Witzel T, Cohen-Adad J, McNab JA, Keil B, Tisdall MD, Hoecht P, Wald LL, 2013. Pushing the limits of in vivo diffusion MRI for the Human Connectome Project. Neuroimage 80, 220–233. 10.1016/j.neuroimage.2013.05.078. [PubMed: 23707579]

Wang Q, Akram H, Muthuraman M, Gonzalez-Escamilla G, Sheth SA, Oxenford S, Yeh FC, Groppa S, Vanegas-Arroyave N, Horn A, 2021. Normative vs. Patient-specific brain connectivity in deep brain stimulation. Neuroimage 224, 117307. 10.1016/j.neuroimage.2020.117307. [PubMed: 32861787]

Weininger J, Roman E, Tierney P, Barry D, Gallagher H, Murphy P, Levins KJ, O'Keane V, O'Hanlon E, Roddy DW, 2019. Papez's Forgotten Tract: 80 Years of Unreconciled Findings Concerning the Thalamocingulate Tract. Front. Neuroanat 13. 10.3389/fnana.2019.00014. [PubMed: 30837847]

Widge AS, Zhang F, Gosai A, Papadimitrou G, Wilson-Braun P, Tsintou M, Palanivelu S, Noecker AM, McIntyre CC, Rathi Y, 2021. Patient-specific connectomic models correlate with, but do not reliably predict, outcomes in deep brain stimulation for obsessive-compulsive disorder. Neuropsychopharmacology 47 (4), 965. 10.1038/s41386-021-01199-9. [PubMed: 34621015]

Yeh FC, 2022. Population-based tract-to-region connectome of the human brain and its hierarchical topology. Nat. Commun 13 (1). 10.1038/s41467-022-32595-4. Article 1.

Yeh FC, Panesar S, Fernandes D, Meola A, Yoshino M, Fernandez-Miranda JC, Vettel JM, Verstynen T, 2018. Population-averaged atlas of the macroscale human structural connectome and its network topology. Neuroimage 178, 57–68. 10.1016/j.neuroimage.2018.05.027. [PubMed: 29758339]

Yendiki A, Aggarwal M, Axer M, Howard AFD, van Walsum A.M.van C., Haber SN, 2022. Post mortem mapping of connectional anatomy for the validation of diffusion MRI. Neuroimage 256, 119146. 10.1016/j.neuroimage.2022.119146. [PubMed: 35346838]

Zhang Z, Descoteaux M, Zhang J, Girard G, Chamberland M, Dunson D, Srivastava A, Zhu H, 2018. Mapping Population-based Structural Connectomes. Neuroimage 172, 130–145. 10.1016/j.neuroimage.2017.12.064. [PubMed: 29355769]

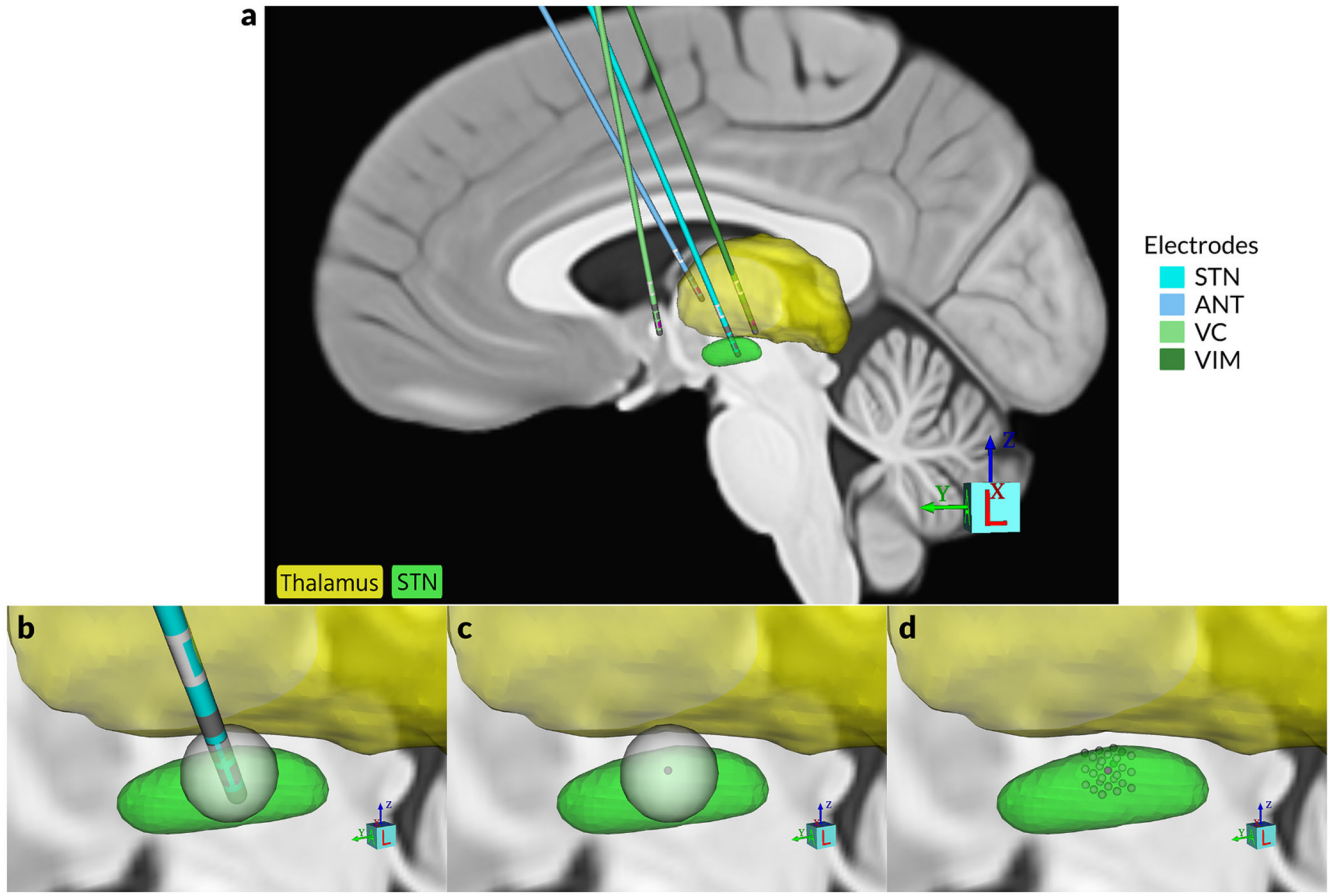

Fig. 1.

DBS targets. (a) Electrode placement for each of the four DBS targets localized within the CIT168 standard brain. (b) Streamline activation was estimated using overlap with a spherical activation volume (shown here for an example activation volume radius of 3 mm at the STN target). (c) The center of the activation volume was coincident with the center of the active contacts of the electrode. (d) A 3 × 3 × 3 grid of 27 points, each spaced 1 mm apart, is used to simulate the effects of electrode location uncertainty for each DBS target.

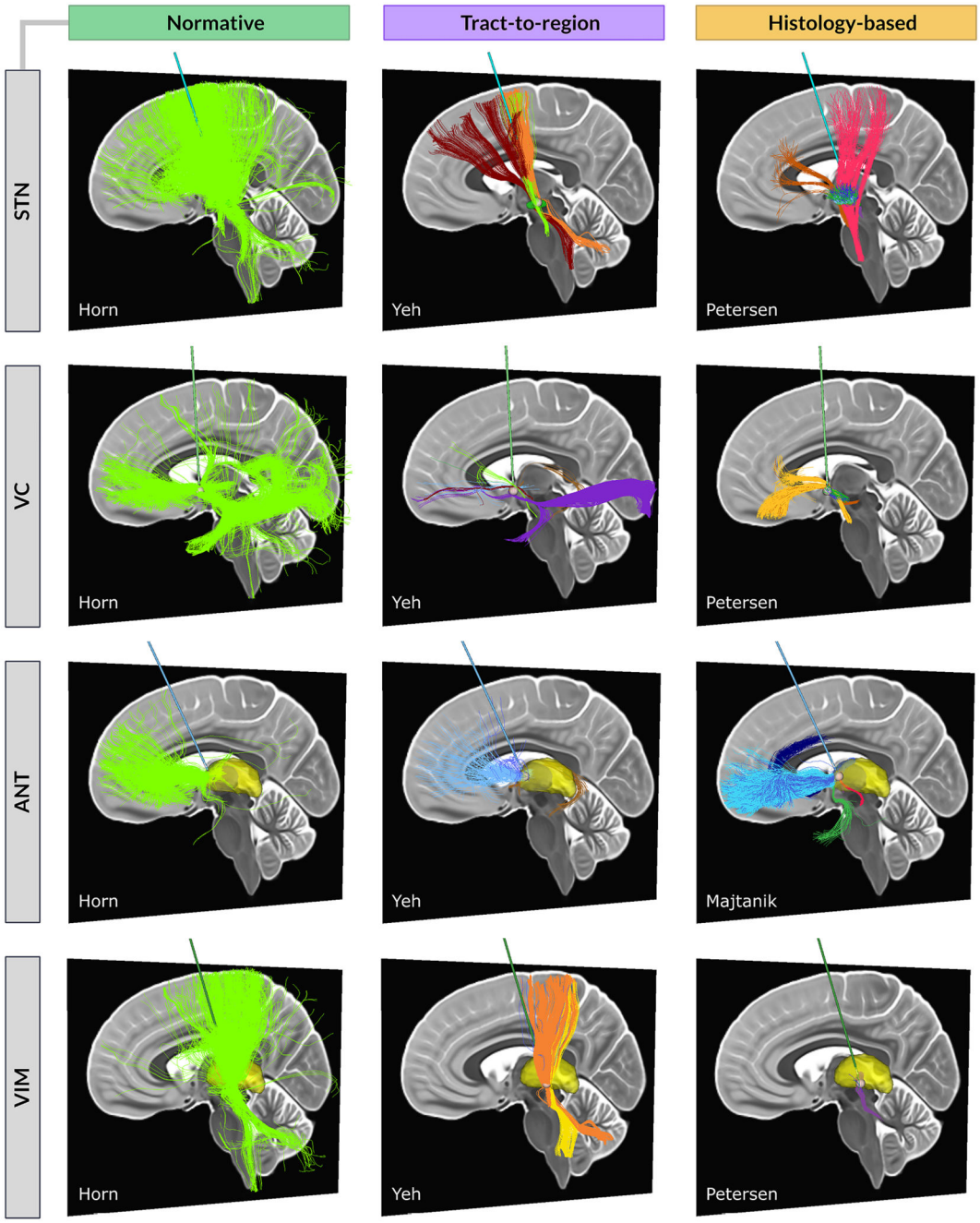

Fig. 2.

Pathway activation. Side-by-side comparison of activated streamlines for each connectome and DBS target location, for an activation sphere of 3 mm centered at the stimulation site.

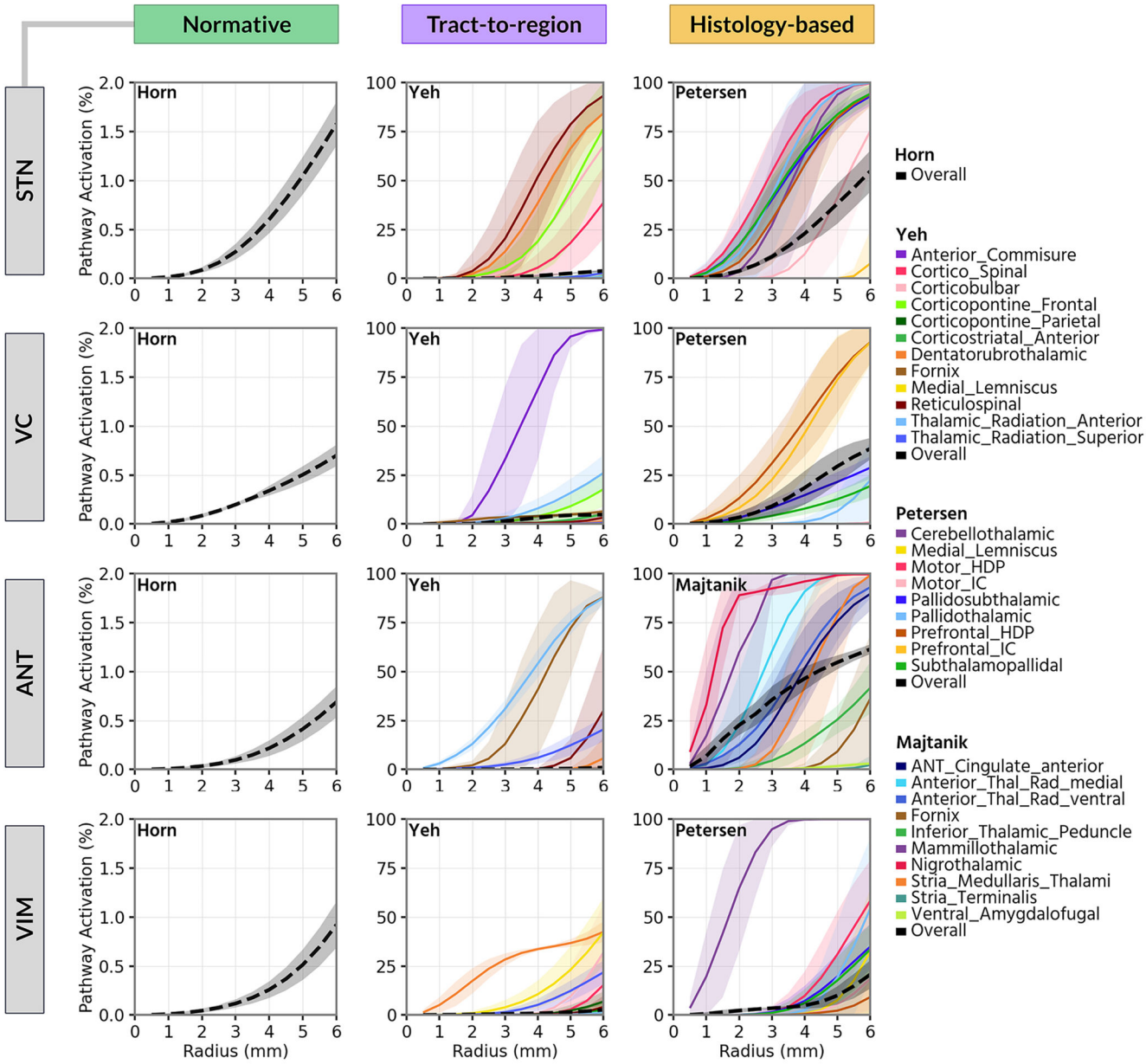

Fig. 3.

Pathway recruitment. Pathway activation at each DBS target location, as a function of the radius of the activation sphere. The dashed black line denotes the overall percentage of streamlines activated in each connectome, averaged over all 27 points, with the shaded region depicting the standard deviation. The solid color-coded lines denote the percentage pathway activation averaged over all 27 points.

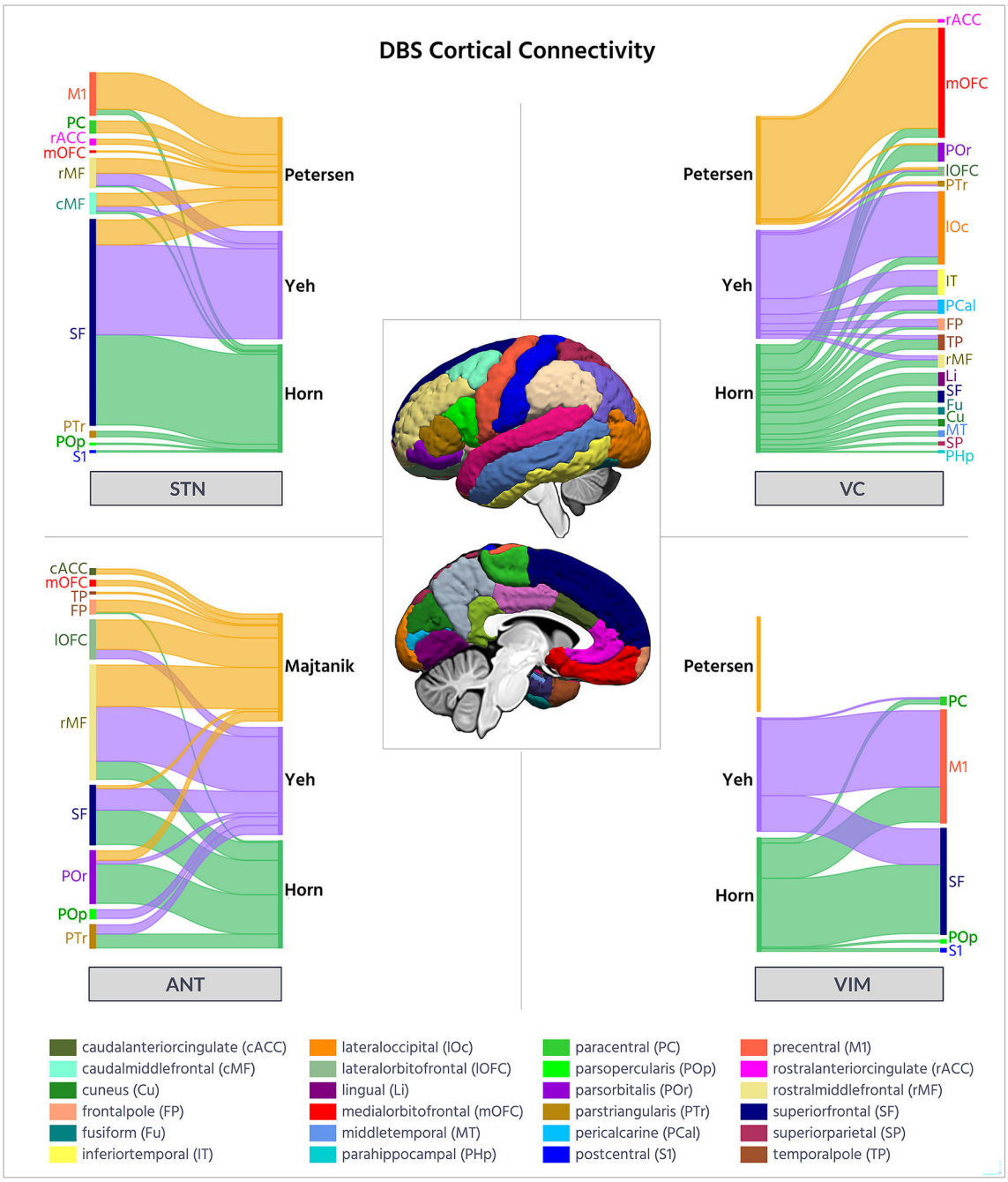

Fig. 4.

Cortical connectivity. Connectivity profiles for each DBS target location, showing the proportion of activated streamlines in a connectome that terminated within that particular ROI (for a 3 mm activation sphere). Central panel: cortical parcellation of the CIT168 brain into 34 ROIs.

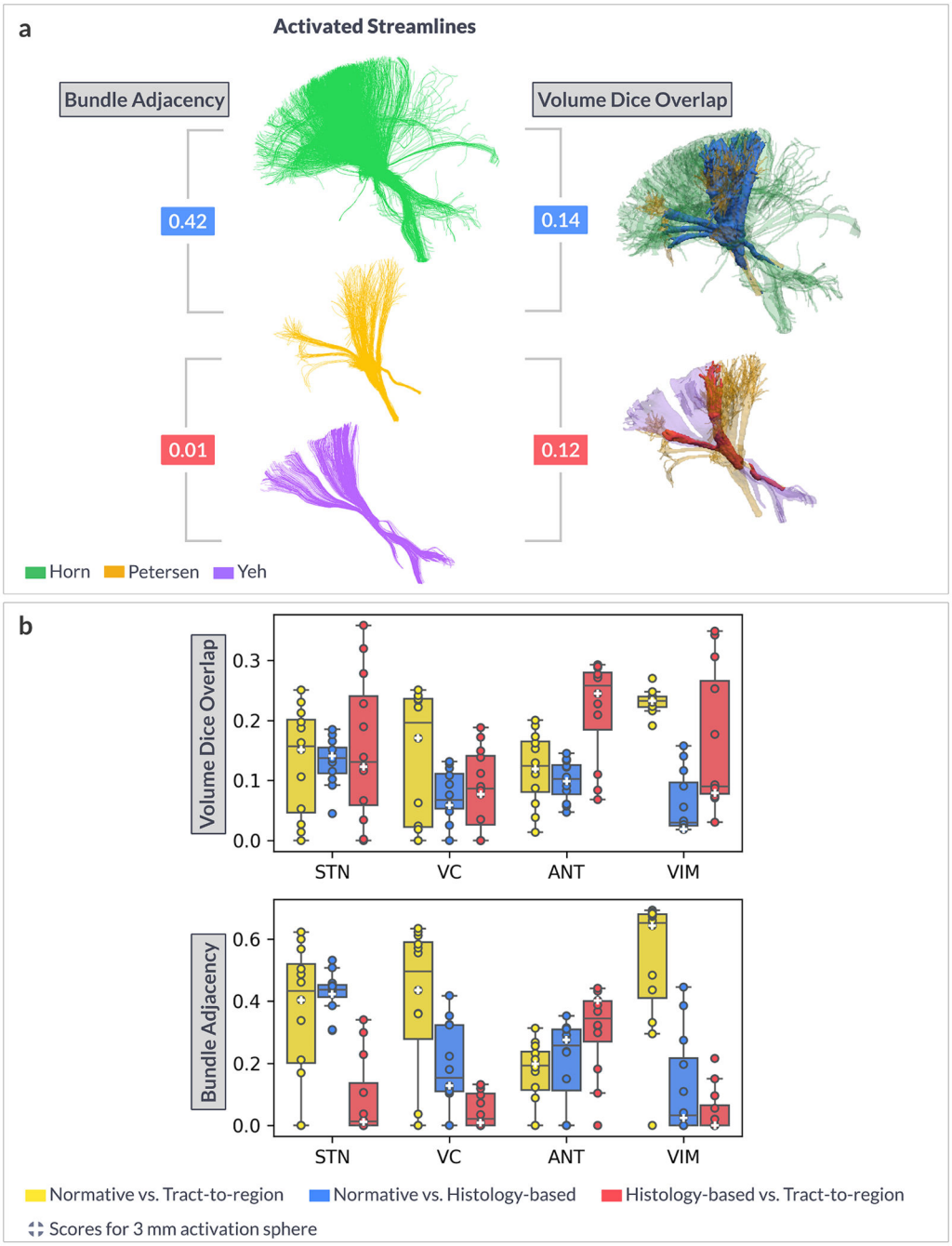

Fig. 5.

Volume Dice overlap and bundle adjacency. (a) Example illustrating the volume Dice overlap and bundle adjacency between Petersen vs. Horn (top), and Petersen vs. Yeh (bottom), for STN DBS and an activation sphere of 3 mm. (b) Box-and-whisker plots comparing the similarity between normative, tract-to-region, and histology-based connectomes across all DBS target locations. Each individual data point on the box plot corresponds to a different activation sphere radius (0 to 6 mm in steps of 0.5, resulting in a total of 12 points per box).

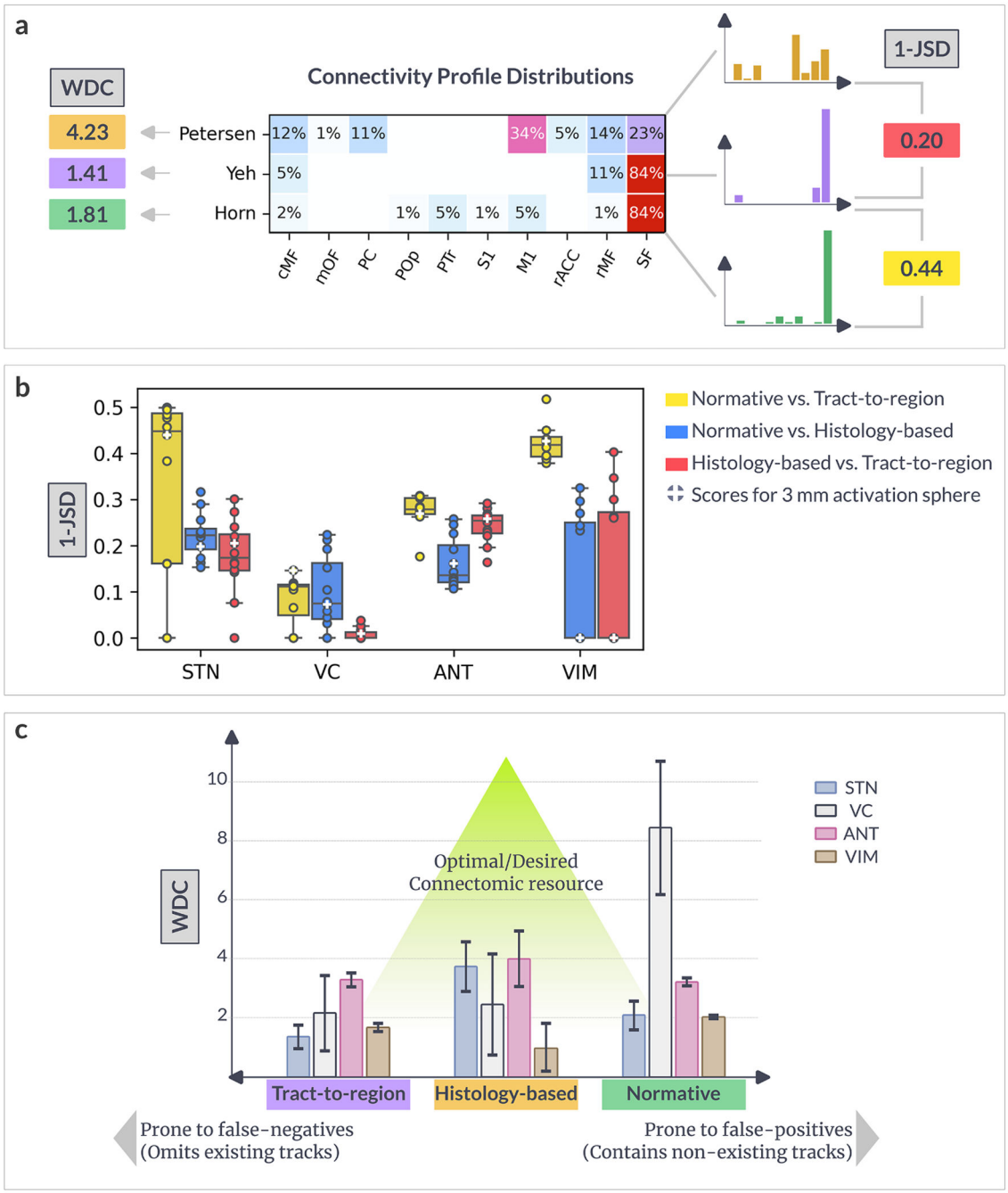

Fig. 6.

Jensen-Shannon distance (JSD) and weighted degree centrality (WDC). (a) Example illustrating the JSD between the connectivity profile of Petersen vs. Yeh (top-right), and Yeh vs. Horn (bottom-right), for STN DBS and an activation sphere of 3 mm. Also, shown are the WDC scores for each connectome (left). (b) Box-and-whisker plots comparing the JSD between normative, tract-to-region, and histology-based connectomes across all DBS target locations. Each individual data point on the box plot corresponds to a different activation sphere radius (0 to 6 mm in steps of 0.5, resulting in a total of 12 points per box). (c)

Variation in WDC scores between DBS targets (mean ± SD; averaged across the entire range of activation sphere radii) grouped together by connectome type. Depicted on the X-axis is the assumed reliability of each connectome.

Table 1

Characteristic features of the connectomic atlases analyzed.

	Horn	Yeh	Petersen	Majtanik
Type	Normative connectome	Tract-to-region pathway atlas	Histology-based pathway atlas	Histology-based pathway atlas
Construction methodology	Population-averaged tractography	Population-averaged tractography with hierarchical clustering	Synthetic reconstruction	Synthetic reconstruction
Sample population	32 young adult HCP	1065 adult HCP	-NA-	-NA-
Scale/Region	Whole-brain	Whole-brain	STN focused	ANT focused
Template space	MNI-ICBM2009b	MNI-ICBM2009a	CIT168	MNI-ICBM2009b
Software	LeadDBS	DSI Studio	StimVision	MRtrix3
File format	.mat	.trk	.vtk	.tck
No. streamlines (left-hemisphere only)	1,863,012	225,551	14,300	14,390

Table 2

Three generalized locations for DBS electrode placement. Coordinates of x (lateral), y (posterior), z(ventral) are in mm relative to the mid-commissural point in AC-PC space within the CIT168 brain.

DBS Target	Indication	Central Stimulation Site		
		x	y	z
Subthalamic nucleus (STN)	Parkinson's disease	−9.6	−1.8	−2.9
Ventral capsule (VC)	Obsessive-compulsive disorder	−9.0	13.6	2.2
Anterior nucleus of thalamus (ANT)	Epilepsy	−5.4	4.8	8.7
Ventral intermediate nucleus of thalamus (VIM)	Essential Tremor	−11.7	−5.0	2.2